JOURNAL OF CATALYSIS 82, 404–417 (1983)

Photoassisted Heterogeneous Catalysis: The Degradation of Trichloroethylene in Water

ANN LORETTE PRUDEN[1] AND DAVID F. OLLIS[2]

Department of Chemical Engineering, Princeton University, Princeton, New Jersey 08540

Received July 28, 1982; revised February 4, 1983

The complete mineralization of trichloroethylene (Cl_2CCClH), in dilute aqueous solutions, to HCl and CO_2 is demonstrated with heterogeneous photoassisted catalysis using illuminated titanium dioxide (TiO_2). An intermediate, dichloroacetaldehyde, is identified, and a photoassisted reaction sequence is proposed. A simple Langmuirian rate equation satisfactorily represents both the disappearance of initial reactant, trichloroethylene, and intermediate, dichloroacetaldehyde, as well as the inhibitory influence of product HCl. The present paper and two related reports (A. L. Pruden and D. F. Ollis, *Environ. Sci. Technol.*, in press; C.-Y. Hsiao, C.-L. Lee, and D. F. Ollis, *J. Catal.* **82,** 418 (1983)) establishing mineralization of chloromethanes, indicate some potential for removal of the two most common chlorocarbon contaminants from water via heterogeneous photocatalysis.

INTRODUCTION

The widespread presence of chlorinated hydrocarbons in both natural and drinking waters of North America (*1, 2*) and Europe (*3*) poses a potentially serious environmental problem, since such ubiquitous halocarbons as trichloroethylene (TCE) and chloroform are carcinogenic and/or toxic (*4, 5*). Both chemicals are classified as "priority pollutants" by the U.S. Environmental Protection Agency (*6*). Such chemicals enter the environment not only through domestic and industrial discharge of solvents (including trichloroethylene) and application of pesticides, but, perversely, through formation of chloroform and other haloforms during conventional water sterilization with chlorine (*7*). A chemical process for degradation of trace halocarbon contaminants ideally should yield innocuous products such as the carbon dioxide and hydrochloric acid expected from complete mineralization. Since toxicity of chlorinated aliphatic hydrocarbons decreases with decreasing chlorine content (*8*), even partial degradation with dehalogenation may provide a partial detoxification.

The objective of our research was to examine the degradation or detoxification of pertinent chlorinated hydrocarbons by photoassisted heterogeneous catalysis and to investigate the kinetics of such reactions. The present paper examines the kinetics of trichloroethylene degradation to HCl and CO_2 by the photoassisted heterogeneous catalyst, titanium dioxide. A TCE rate equation is derived which accounts for our experimental observations, and tentative mechanisms for the surface reactions are discussed.

Chloroform ($CHCl_3$), a common synthetic product arising during municipal chlorination of drinking water supplies, is also fully mineralized by heterogeneous photocatalysis (*10*); a discussion of chloromethane photocatalyzed mineralization follows (*60*).

[1] Present address: Mobil Research & Development Laboratory, Pennington, N.J.

[2] Present address: Chemical Engineering Department, University of California, Davis, Calif. 95616.

0021-9517/83 $3.00

Prior suggestions of catalytic dehalogenation activity of illuminated semiconductors exist. A qualitative report of polychlorinated biphenyl (PCB) dechlorination (*11*) in the presence of uv-illuminated TiO_2 noted only reactant disappearance and chloride presence; intermediates were not mentioned. The total amount of PCB converted corresponded to only 2×10^{-3} of a monolayer on TiO_2, leaving open the question of whether the solid surface functioned as a catalyst or as a reagent (*12*). Illumination of uncharacterized sediments thought to contain semiconductor oxide in clay components brought no noticeable conversion of *p*-dichlorobenzene (*p*-DCB) (*13*), but illuminated 1 wt% anatase (TiO_2) slurries in water resulted in *p*-DCB disappearance with a reported half-life of 5 min. No reaction products were identified, nor was dehalogenation actually demonstrated. Aromatic hydrocarbons and chlorinated alkenes were partially photomineralized to CO_2, HCl, and Cl_2 when adsorbed on silica gel and irradiated with quartz- or Pyrex-filtered uv light in oxygen (*14*). No uv spectra of silica gel are contained in standard compilations, implying that silica gel does not absorb in the uv. Therefore, photoassisted catalysis at uv and near-uv wavelengths (200–400 nm) would occur only by excitation of impurities in the solid; also, it is possible that the Cl_2 and HCl observed were produced by direct photochemical dehalogenation by uv photons (*15*).

EXPERIMENT

The reactions were carried out in a batch reactor (Fig. 1) constructed of glass and Teflon. A 0.1 wt% aqueous slurry of titanium dioxide was recirculated with a polypropylene/ceramic pump. The catalyst was Fisher Certified grade TiO_2, Lot #745547, with a surface area of 7 m^2/g, as determined by BET nitrogen adsorption (*16*). The predominant (~95%) crystalline modification was anatase, as determined by X-ray diffraction (*17*). Trichloroethylene was Baker

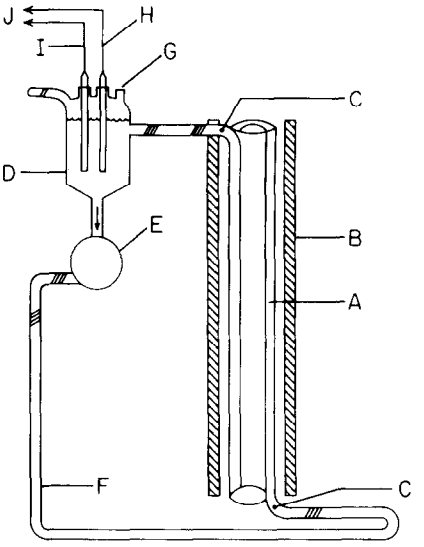

FIG. 1. Recirculating, differential conversion photoreactor. (a) Quartz annular photoreactor; (b) Black lights parallel to reactor axis (7 GE BLB (15 W)); (c) thermocouple; (d) Pyrex sampling vessel; (e) centrifugal recirculation pump; (f) Teflon tubing; (g) sampling port with Teflon-faced septum; (h) chloride ion electrode; (i) reference electrode; (j) millivoltmeter.

Analyzed reagent grade, used without further purification.

Freshly boiled distilled deionized water, stripped with helium in the reactor to further remove dissolved oxygen and carbon dioxide, was used in all runs. Thus the oxygen concentration in the water was far less than 7 ppm O_2, the equilibrium value for air-saturated water at 30°C (*18*). (The oxygen content of nitrogen-purged water at 5–40°C was measured earlier with a dissolved oxygen probe to be $\sim 2 \times 10^{-5}$ *M*, or 0.6 ppm (*19*). At the end of several experiments, the slurry was again stripped with helium, and the gaseous effluent bubbled through a saturated barium hydroxide solution to trap carbon dioxide. Appearance of the barium carbonate precipitate (solubility of 0.002 g/100 ml at 18–20°C (*20*)) confirmed the formation of carbon dioxide during the reaction. These precipitates could not be due to formate production since the solubility of barium formate is 27.8 g/100 ml (*20*)).

The slurry was recirculated through a quartz annular reactor illuminated by seven commercial black light fluorescent bulbs (GE BLB—15 W) arranged parallel to the reactor axis (Fig. 1). The total fluid volume was ~625 cm^3; the illuminated volume, 300 cm^3; the volumetric flow rate, 40 cm^3/sec. Thus each fluid element spent 7.5 sec per pass, or about half the total reaction time, under illumination. The annular radius was 1.65 cm, with a cross-sectional area of 8.1 cm^3, yielding a linear velocity in the illuminated volume of ~5 cm/sec. The black lights emitted predominantly 320–440 nm light, with virtually no emission below 300 or above 500 nm. These lamps were chosen to maximize emission in the TiO_2 absorption spectrum (*21*) while eliminating wavelengths more energetic than 3000 Å as the latter can drive homogeneous photochemical reactions, including dehalogenations (*15*). The uv-absorption spectrum of TCE shows a molar extinction coefficient, ε, of less than 10 liters/mol · cm above 260 nm, or an absorbance (*22*), A, of less than 4.5×10^{-3} for a TCE concentration of 50 ppm and a path length of 1.3 cm.

Potassium ferrioxalate actinometry (*23*) in TiO_2-free solutions was used to measure the near-uv intensity entering the reactor. The overall photochemical reaction was

$$2Fe^{3+} + C_2O_4^{2-} \xrightarrow{h\nu} 2Fe^{2+} + 2CO_2$$

Ferrous ion was complexed with *o*-phenanthroline, and the absorbance measured at 510 nm with a Cary 14 spectrophotometer. The quantum yield of ferrous ion and molar extinction coefficient of the ferrous–phenanthroline complex are well established (*24*); values of 1.21 and 1.11×10^4 liters/mol · cm were used here. The chemical actinometer, prepared as needed by mixing standardized solutions of 1.2 *M* $K_2C_2O_2$ and 0.2 *M* $Fe_2(SO_4)_3$ to form 0.02 *M* $K_3Fe(C_2O_4)_3$, was irradiated as it circulated through the reactor. From the absorbance of the ferrous complex per unit time, the photon absorption rate in the reactor was calculated as 6.6×10^{-4} Einsteins/min. The actinometer measured the total photon rate entering the reactor. During subsequent catalyst studies with TiO_2 suspensions in actinometer-free solutions, scattering losses, if any, due to the syspended TiO_2 were not accounted for. Thus, the calculated quantum yields reported later in this paper are minimum values.

The absorption efficiency of the reactor, defined as the ratio (photons absorbed (actinometer measurement)/photons emitted by lamp based on manufacturer's specification) × 100 was found to be 22%.

Addition of TCE to the water-filled reactor was made by microsyringe (5–50 μl) injections. A saturated solution of TCE at 20–25°C and 1 atmosphere contains 1.1×10^3 mg TCE/liter, or about 1100 ppm (*6*). Organic reactants and products were followed by analysis with a Perkin-Elmer Sigma 1 gas chromatograph on a Tenax column (60/80 mesh, 1 m × ⅛ in. o.d., nickel) followed by flame ionization detection at 120°C (isothermal). The volatile reactant, TCE, was determined by analysis of the headspace vapor over 1 ml liquid sample contained in 1 dram vials capped with Teflon-faced silicone septa. Following Piet *et al.* (*25*), at least 45 min were alloted for TCE equilibration between the liquid and vapor phases. The composition of the vapor phase was stable between 45 min and 12 hr as long as the septum had not been punctured previously. Analyses of the liquid phase directly for TCE were unreliable, due to major evaporation of TCE into the headspace. Dissolved organic products were monitored by GC analysis of direct chromatograph injection of the aqueous phase, following centrifugation of suspended TiO_2 particles.

Chloride ion production was followed *in situ* with a specific chloride electrode (HNU Systems and Orion Model 801 pH/mV meter). The electrode was calibrated with HCl solutions, rather than ionic strength adjustor, to account automatically for the related pH decrease observed during chloride evolution without adding other ions to the reaction mixture. Agreement be-

tween final chloride values so determined and subsequent silver nitrate titration (Mohr's method) (*26, 27*) was within 2%.

The fluid temperature was measured at the inlet and outlet of the illuminated quartz vessel with Fluke Model 2166A Digital Thermometer and Omega matched iron-constantan thermocouple (*28*) (wire diameter 0.010 in. Teflon casing 0.003 m) taped to the quartz. The maximum fluid temperature difference between reactor top and bottom after prolonged illumination was 5°C; the average temperature is reported here.

TABLE 1

TCE Conversion to Chloride

Initial TCE (ppm) run No.		Equivalent Cl^- Fed (ppm)	Maximum Cl^- observed (ppm)[a]	Conversion of Cl^- (%)
E_1	10.3	8.3	5.0	
E_2	23.6	19.1	16.3	
E_3 =	46.7	37.8	42.3	
	80.6	65.2	63.6	98
F	45.9	37.2	36	97
G	45.4	36.8	37	100.5

RESULTS

Neither TCE disappearance nor chloride appearance were noted during 2 hr illumination of a catalyst-free reactor. The results of a characteristic TCE degradation experiment, with successive injections of TCE, are shown in Fig. 2. In the simultaneous presence of TiO_2 and illumination, trichloroethylene was continuously dehalogenated. Chloride production stopped immediately when the lamps were turned off. At an initial TCE concentration of ~10 ppm, only chloride product was observed in the bulk liquid; no organic product was detected. At higher levels (24 and 47 ppm), production and consumption of an intermediate identified by GC-MS (*24*) as dichloroacetaldehyde (Cl_2HCCHO) was observed, with continued chloride production. This intermediate, DCA, was water soluble and stable in the dark in solutions containing TiO_2 particles for several months.

During TCE degradation experiments, the pH fell to typical levels of ~4.0–6.8, depending on the amount of TCE converted. No gas evolution was observed, nor were any other products detected by GC in either the gas or liquid phase. Carbon dioxide presence in the reacted solution was demonstrated by the appearance of barium carbonate following passage of a helium stripping stream into a barium hydroxide solution. The chloride mass balances for experiments in which both TCE and DCA decreased to levels undetectable by GC-FID (<500 ppb for TCE) are presented in Table 1. Essentially all (97–100.5%) of the chlorine fed as TCE was recovered as chloride ion in solution (last column, Table 1).

Initial TCE and Cl^- concentrations for each run appear in Table 2 with initial reaction rates. Specific activities (column 4), photoassisted specific activities (based on photons entering the reactor) (column 5), and turnover numbers (column 6) were calculated from measured initial rates (initial slope × initial concentration). The apparent first-order rate constants (initial slopes of ln(TCE) vs time) are shown in the last column.

The apparent first-order reaction rate constant eventually decreased for initial TCE concentrations of 47 ppm and greater, as shown in Figs. 2 and 3. Addition of chloride as HCl to the initial reaction mixture of Fig. 3 resulted in a decrease in the apparent rate constant, as noted in Table 2. Addition of the carbon dioxide equivalent of more than 100 ppm TCE conversion had no effect. The intermediate DCA was not commercially available, and was not tested as an inhibitor.

Product DCA disappearance also proceeds in apparent first-order fashion after the TCE has been consumed, as evidenced

TABLE 2

Rates for TCE Conversion (36–38°C)

Run No.	Initial concentration TCE (ppm)	Initial concentration Cl^- (ppm)	Specific activity[a] (μmol/cm^2 · min) ($\times 10^{-4}$)	Turnover number[b] (molecules/site · s) ($\times 10^{-2}$)	Specific rate/ photon absorbed[c] (μmol/cm^2 · min · μmol photon) ($\times 10^{-6}$)	Apparent first-order rate constant k_{TCE}(min^{-1})
E1	10.3	1.5	4.1	0.9	0.6	0.365
E2	23.6	6.3	9.4	1.9	1.4	0.352
E3	46.7	20.7	10.9	2.3	1.9	0.214
C	45.4	2.5	18.0	3.7	2.7	0.353
F	45.9	126.0	9.7	2.0	1.5	0.198

[a] Based on measured surface area, 7 m^2/g.
[b] Based on assumed surface site concentration of 5×10^{14} sites/cm^2.
[c] Based on photons absorbed by the actinometer, 660 μmol/min.

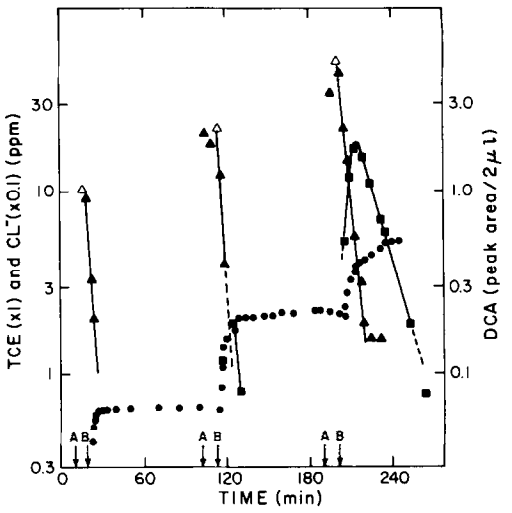

FIG. 2. Photocatalyzed degradation of trichloroethylene. Arrows (↓): A, no illumination, TCE injection; B, illumination *on*. Concentrations: (△) trichloroethylene (calculated); (▲) trichloroethylene (measured); (●) chloride ion (measured); (■) dichloroacetaldehyde (measured).

by the straight-line decay (Figs. 2 and 3) on semilog plots.

Since the calibration was not available for DCA, its production was calculated from a chlorine mass balance, assuming

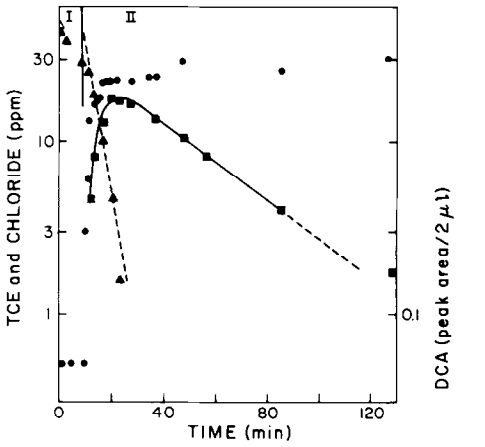

FIG. 3. Chloride ion inhibition test. Initial concentrations: trichloroethylene, 45.9 ppm; chloride (as HCl), 145 ppm. Data: (△) TCE (calculated); (▲) TCE (measured); (●) chloride ion (produced): (■) DCA measured. Regions: I. catalyst, no illumination; II. catalyst and illumination.

that the chlorine initially charged to the reactor is conserved as either unreacted TCE, chloride ion, or DCA. The calibration proportionality constant between measured DCA peak area and calculated DCA was determined at the point of maximum measured DCA level. The concentrations of DCA (integrated peak area per 2 μl sample) calculated after TCE was consumed, the corresponding chloride levels, and apparent first-order rate constants for DCA disappearance are shown in Table 3. The specific rates (peak area per 2 μl of injection per unit catalyst weight) are independent of reaction order.

The DCA concentrations calculated for the final portion of Fig. 3 are compared in Fig. 4 to the corresponding peak areas observed in solution. The difference between total DCA production (calculated) and DCA concentration measured in solution implies that this intermediate may be strongly bound to the catalyst surface.

The specific activities (μmol · cm^{-2} min^{-1}) for TCE and DCA conversions in Tables 2 and 3 are similar to those which we calculated from literature reports which appear to involve other heterogeneously photocatalyzed reactions (*12*). All show turnover numbers near 10^{-2} sec^{-1} if a fully active surface (5×10^{14} sites cm^{-2}) is assumed. Based on the highest amount of TCE converted (660 ppm), as computed from a chlorine mass balance, the turnovers accomplished were 87 for TCE conversion and 261 for chloride production, indicating the catalytic nature of this reaction (*12*).

The highest initial quantum efficiency ((moles TCE converted per mole photon absorbed by actinometer solution) × 100) observed in this study was 1.7%. The lesser levels typifying Figs. 3–5 were 0.3–0.9%.

DISCUSSION: KINETICS

The disappearance of TCE and DCA below detectable limits, the lack of other observable organic products by GC or GC-MS, the observation of carbon dioxide formation and the demonstration of a chlo-

TABLE 3

Rates of Dichloroacetaldehyde Conversion (39–40°C)

Run No.	DCE[a] Concentration (P.E. counts)	Concentration Cl^- (ppm)	Rate (P.E. counts/g-cat/min)	Specific activity[b] (μmol/cm^2 · min) ($\times 10^{-5}$)	Turnover number (molecules/site · s) ($\times 10^{-2}$)	Specific rate/photon absorbed (μmol/cm^2 · min μmol photon) ($\times 10^{-8}$)	Apparent first-order rate constant k_{DCA} min^{-1}
C	1.1764	35	0.1301	2.3	2.9	3.5	0.069
E_3	1.111	45	0.1104	2.0	2.4	3.0	0.060
F	1.0546	158	0.0447	0.8	1.0	1.2	0.026

[a] At time when (TCE) below detection; P.E. counts = peak area/2 μl injection.
[b] Estimated from calibration factor of Fig. 10; 20 ppm DCE = 1.6 P.E. counts.

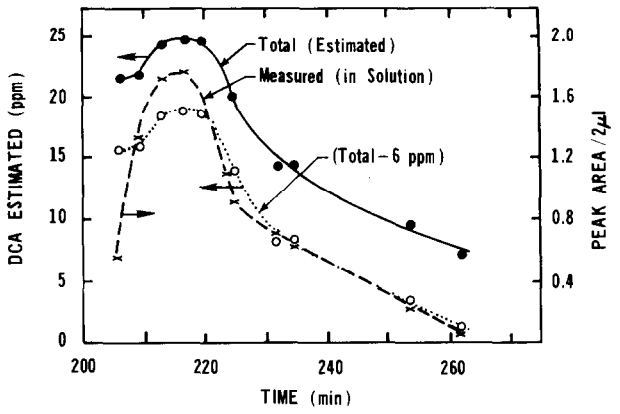

FIG. 4. Dichloroacetaldehyde vs time. Dichloroacetaldehyde calculated from chlorine balance (●): (calculated value—6 ppm, ○); (measured value, X). Note: 6 ppm is approximately 0.9 monolayers of DCA.

ride mass balance combine to show for the first time the essentially complete degradation of trichloroethylene and of dichloroacetaldehyde to inorganic products by photoassisted heterogeneous catalysis.

To analyze the observed kinetics of this novel degradation, we consider first the development of an "active" surface when the illumination is begun. The lifetime of a photogenerated hole ranges from 10^{-19} to 10^{-3} sec (*30*), and the diffusion time of a photogenerated hole across the space-charge region in n-TiO_2 was calculated to be on the order of 10^{-14} sec (*31*). The slopes of the TCE data (Table 2) indicate a reaction time ($1/k_{app}$) of the order of 10^2 sec. Thus, the surface, upon illumination, will come rapidly to an active steady state including photo-produced holes, i.e., the relaxation time for the solid is so fast that we do not expect our kinetic data for TCE to reflect any transient condition of the photoactivation.

Another potentially rate-limiting step might be TCE mass transfer to the photoactivated surface. Such a circumstance would arise only if the near surface TCE concentration were essentially zero (rapid reaction limit). From a mass transfer calculation, the maximum possible liquid–solid mass transfer rate was 10^4 times the observed reaction rate. These values show that the surface catalytic reaction must be the slow step in this conversion, as both solid state and liquid film transport processes are much too rapid to be a major pseudo-steady-state kinetic resistance.

A Simple Kinetic Model

The specific rate for apparent first-order surface decomposition of TCE at constant intensity with chloride competition for the active site may be expressed, for simplicity, in terms of Langmuir–Hinshelwood kinetics as

$$-r_{TCE} = k_{TCE}\theta_{TCE} \qquad (1)$$

where the surface coverage of TCE, θ_{TCE}, is

$$\theta_{TCE} = \frac{K_{TCE}\theta_{TCE}}{1 + K_{TCE}[TCE] + K_{Cl}[Cl]}. \qquad (2)$$

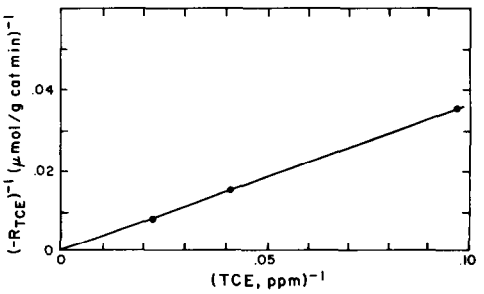

FIG. 5. Reciprocal rate vs reciprocal TCE concentration. Initial chloride: less than 7 ppm.

The adsorption coefficients K_{TCE} and K_{Cl} are functions of temperature (and perhaps intensity in photoassisted heterogeneous reactions), but are assumed constant throughout our nearly isothermal reactor. The surface rate constant, k_{TCE}, defined by Eq. (1) (also a function of temperature and intensity), is similarly assumed constant. The concentrations of TCE and chloride are the bulk fluid concentrations.

Inversion of the rate obtained from Eqs. (1) and (2) allows evaluation of the constants from the data of Table 2. The inverted equation may be plotted in two ways to allow evaluation of all three constants from slopes and intercepts of the plots, i.e.,

$$\frac{1}{r_{TCE}} = \frac{1}{k_{TCE}}\left[\frac{1}{K_{TCE}} + \frac{K_{Cl}[Cl]}{K_{TCE}}\right]\frac{1}{[TCE]} + \frac{1}{k_{TCE}} \quad (3a)$$

and

$$\frac{1}{r_{TCE}} = \frac{1}{k_{TCE}}\left[\frac{K_{Cl}}{K_{TCE}[TCE]}\right] \times [Cl] + \left[\frac{1}{k_{TCE}K_{TCE}[TCE]} + \frac{1}{k_{TCE}}\right]. \quad (3b)$$

For chloride levels below 6.3 ppm, Table 2 shows the first-order rate constant to be independent of chloride concentration, implying that $K_{Cl}[Cl]$ is small compared to unity, and that the slope of Eq. (3a) may be approximated as

$$\text{slope} \simeq \frac{1}{k_{TCE}K_{TCE}}.$$

A plot of inverse rate versus inverse TCE concentration, at low chloride levels (Fig. 5), is linear as predicted by Eq. (3a). The intercept determines k_{TCE}, then K_{TCE} can be calculated from the previous slope approximation.

For inhibitory chloride levels (greater than 20.7 ppm), a plot of inverse rate versus chloride concentration at constant TCE concentration (Fig. 6) is plausibly linear, as predicted by Eq. (3b). Using the value of k_{TCE} from Fig. 4, K_{Cl} and K_{TCE} can be determined from the slope and intercept of Fig. 5. The values of the constants of Eqs. (2) and (3) calculated from these relationships are k_{TCE} = 830 ppm TCE/(min-g · cat), $K_{TCE} = 4.0 \times 10^{-4}$ ppm^{-1}, and $K_{Cl} = 4.8 \times 10^{-3}$ ppm^{-1}. The value for K_{Cl} of $\sim 5 \times 10^{-3}$ ppm^{-1} compares favorably with that for iodide ($K_I = 2.5 \times 10^{-3}$ ppm^{-1}) estimated from rate measurements on an illuminated TiO_2 slurry under similar conditions (*32*).

The DCA appears to be strongly bound to the catalyst, as suggested by the discrepancy between calculated and observed DCA concentrations previously discussed. The difference between calculation (based on Cl balance) and measurement is approximately constant in the latter stages of reaction, as indicated in Fig. 4; it corresponds to approximately 6 ppm DCA, or about 0.9 monolayer of DCA on a surface of 5×10^{14} sites/cm^2.

Inhibition of DCA mineralization is also evident. In Fig. 6, we plot the inverse DCA rate calculated from the slopes in Figs. 2 and 3 when the DCA chromatograph peak area = 1.11 units/2 μl; this fixed DCA concentration at very low TCE levels allows use of Eqs. (3a) and (3b) to evaluate the corresponding rate parameters. The linear plot obtained in Fig. 6 indicates that a simple Langmuir inhibition model appears to suffice.

The Fig. 6 DCA data suggest a simple Langmuir equation for DCA analogous to that for TCE:

$$\text{rate} = \frac{k_{DCA}K_{DCA}[DCA]}{1 + K_{DCA}[DCA] + K_{Cl}[Cl]} \quad (4)$$

with the slope and intercept for Fig. 6 given by

$$\frac{1}{\text{rate}} = \frac{1}{K_{DCA}}\left[1 + \frac{1}{K_{DCA}[DCA]}\right] + \left[\frac{K_{Cl}}{K_{DCA}[DCA]}\right][Cl^-] \quad (5a)$$

$$= (\text{intercept}) + (\text{slope})[Cl^-]. \quad (5b)$$

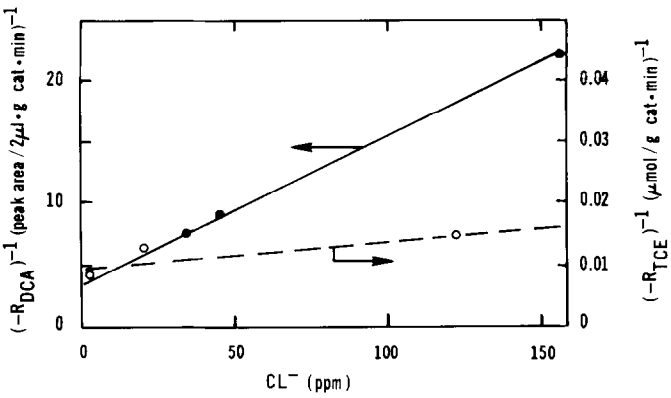

FIG. 6. (Dashed line and data (●) for reciprocal initial rate vs initial chloride concentration. Reciprocal DCA rate vs chloride concentration (solid line and data (○)). Initial DCA level = constant (peak area) = 1.11 units/2 μl (Figs. 3 and 4).

The slope and intercept values provide two equations relating the three variables k_{DCA}, K_{DCA}, and K_{Cl} at a fixed concentration of [DCA] = 13.8 ppm (1.11 peak area units/2 μl sample). A third data point far removed from this DCA value, and the corresponding rate value, provides the third relation between these rate equation parameters, and gives the parameter values $k_{DCA} = 4.44 \times 10^3$ μmol DCA/(min-g · cat.), $K_{DCA} = 0.25$ ppm^{-1}, and $K_{Cl} = 0.145$ ppm^{-1}.

The considerably stronger apparent inhibition by chloride ion for DCA ($K_{Cl} = 0.145$ ppm) vs TCE ($K_{Cl} \sim 5 \times 10^{-3}$ ppm) suggests that either the DCA is converted on a different site than TCE, and chloride is bound more strongly there, or that a different product is (also) inhibiting the reaction, specifically (H^+). We note here that a similar higher apparent chloride binding (inhibition) constant has been determined in our labs for the saturated, partially chlorinated chloromethanes, CH_2Cl_2 (*60*) ($K_{Cl} = 2.47 \times 10^{-2}$ ppm) and $CHCl_3$ (*10*) ($K_{Cl} = 0.22$ ppm^{-1}).

These inhibition results appear to be reasonably explained when the nature of the binding of the reactants on the TiO_2 surface is considered. The titania surface has both acidic sites (associated with the coordinative unsaturation of metal at the surface) and basic sites (associated with surface anions or anion vacancies). Surface Ti(III) ions have been observed by ESR (*34, 35*). In the dark they are due to defect sites in the lattice structure; under near-uv illumination their concentration is increased by Ti(IV) reduction by photogenerated electrons. Olefin π-bonds and chloride bonds to Ti(III) are well established in the Ziegler–Natta polymerization of olefins over solid $TiCl_3$ (*36*). Trichloroethylene can adsorb on such a metal site by interaction of π-electrons with the metal. Chloride also would adsorb on such a site (as it does in Ziegler–Natta catalysts also) (*36*) giving rise to adsorption inhibition by chloride product.

The aldehyde DCA, on the other hand, cannot fill the metal ligand vacancy directly upon readsorption from the fluid phase. The equilibrium between the keto-enol structures of aldehydes lies far to the left (*37*) in Eq. (6). The alpha-hydrogen

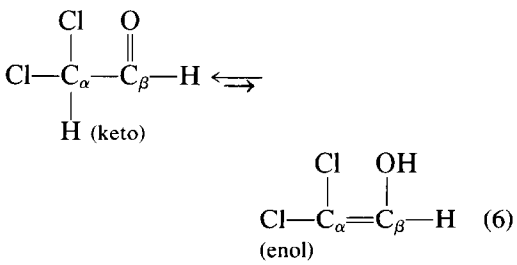

(6)

is weakly acidic by virtue of the electron-withdrawing nature of both the carbonyl

oxygen on the β-carbon and the chlorines on the α-carbon. We may envision the adsorption of DCA as requiring a pair of sites, with the acidic α-hydrogen attracted to a basic site and the remaining fragment to an acidic site. This dual-site adsorption hypothesis for species with an acidic hydrogen is supported by:

(1) the known dissociative adsorption of water on metal oxide surfaces;

(2) the suggestion based on ir adsorption spectra and temperature-programmed desorption experiments (in the dark) that alcohol adsorption on anatase involves hydrogen bonding of the alcoholic (acidic) hydrogen to O^{2-} surface ions and bonding of the remaining fragment to a metal site (*38, 39*);

(3) the suggestion based on product distributions and disappearance of the O-ESR signal that surface alkoxides (RO^-, for R = CH_3, C_2H_5) are formed on uv-illuminated TiO_2 from methane and ethane (*40*);

(4) the two-site mechanism for alcohol dehydration in gas–solid photocatalysis proposed earlier by us gave rate expressions in agreement with kinetic data, whereas a single-site model was unsatisfactory;

(5) the predominance of RH products over R_2 or H_2 products in the aqueous photoassisted decarboxylation of organic acids by TiO_2 (*42, 43*) suggests acid decomposition and alkane formation on adjacent sites.

The dual-site hypothesis implies that, for the degradation of DCA, both chloride and protons, competing for the acidic and basic sites, respectively, can inhibit DCA reaction. The apparent effect of (hydrogen) chloride inhibition could thus be more pronounced than for the single site activation of TCE. Although sufficient data are not at hand to test kinetically the dual-site hypothesis, it *is* plausible on grounds of organometallic bonding and acid–base behavior of oxide surfaces. This hypothesis accounts qualitatively for the observed effect of chloride and accompanying proton production on the rates of degradation of TCE and DCA. It appears that the photocatalyzed degradation of chloroform (CCl_3H) can also be described by such a dual site adsorption (*10*).

Dichloroacetaldehyde Formation

To account for the photoassisted heterogeneously catalyzed nature of the TCE conversion to DCA, we suggest the route to intermediate formation shown in Table 4. The following evidence supports this scheme:

(1) The fundamental event in photoactivation of the solid is Reaction (4-1).

(2) In aqueous solution, the surface of TiO_2 is covered with hydroxyl groups (*44*), as well as molecular water. The hydroxyl groups may react with the photogenerated hole to produce hydroxyl radicals (4-2). These species have been postulated, for example, in the photo-oxidation of isopropanol (*45, 46*) and production of hydrogen peroxide (*47*), and have been verified in the presence of oxygen and illuminated TiO_2 via the production of H_2O_2 (*48*), alcohol scavenging (*13*), and electron spin resonance (*49, 50*).

(3) The substitution of OH for Cl on chlorinated hydrocarbons is known to occur over oxide catalysts at elevated temperatures (*51*). It is reasonable that an activated species such as the hydroxyl radical could attack the C–Cl bond. Subsequent keto-enol tautomerization of the resulting vinyl alcohol is then expected.

(In homogeneous gas phase photochemical studies, trichloroethylene and oxygen in uv light (wavelength unspecified) yielded dichloroacetyl chloride ($Cl_2HCCOCl$) (*52*); that is, no chlorine loss occurred. In the presence of molecular oxygen and simulated solar illumination ($\lambda \geq 300$ nm), no conversion of tetrachloroethylene was observed; however, *in the presence of hydroxyl radical,* dichloroacetylchloride ($Cl_2HCCOCl$) was formed (*53*) (Eq. (7)), analogous to our proposed Eqs. (8a,b) for DCA appearance.)

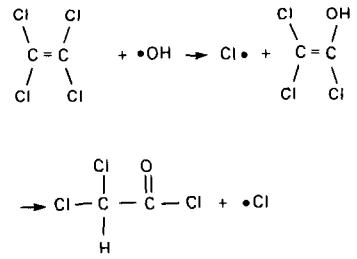

(7)

(4) Adsorption of chloride ion as HCl on illuminated TiO_2 has been shown to decrease the photoadsorptive capacity for oxygen (*54*), which adsorbs as O_2^- by reaction with the photoproduced electron (*55*, *56*). We suggest that on the sites for which chlorine and oxygen compete (the metal sites), the chlorine atom may also react with an electron as in Reaction (4-7). Alternately, Eqs. (4-4) and (4-7) may yield chloride directly. This reaction closes the photocatalytic cycle in the intermediate formation; both the hole and electron have been consumed.

The stability of dichloroacetaldehyde in solution with TiO_2 *in the dark*, as opposed to its complete degradation under continu-

TABLE 4

A Photocatalyzed Route to Dichloroacetaldehyde (Proposed)[a]

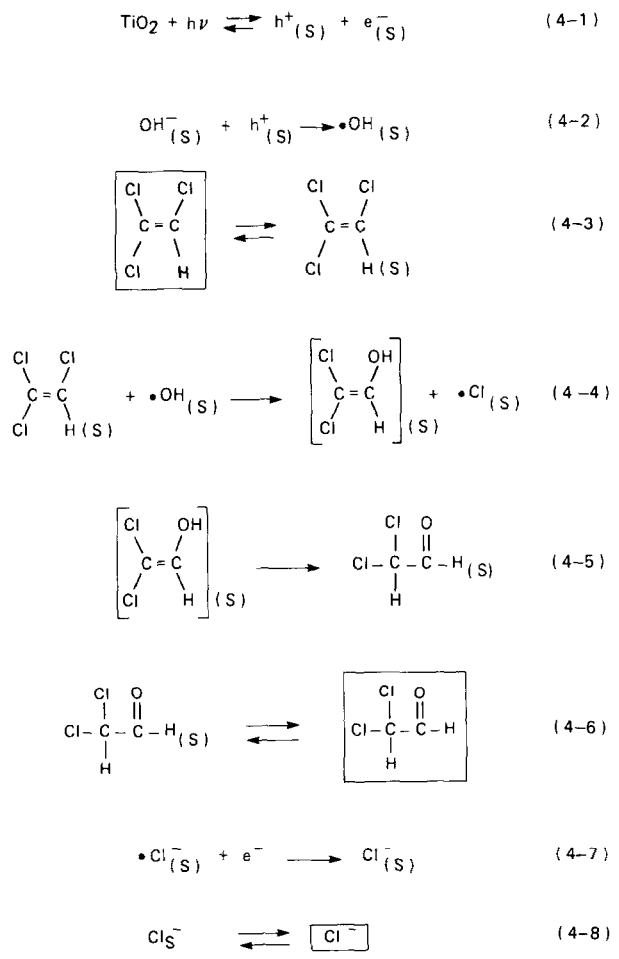

[a] Boxed species were observed in solution.

ing illumination, implicates some photogenerated species in its further degradation. One possibility for breaking the carbon–carbon bond involves formation of dichloroacetic acid ($\bar{V}$) and its subsequent decomposition:

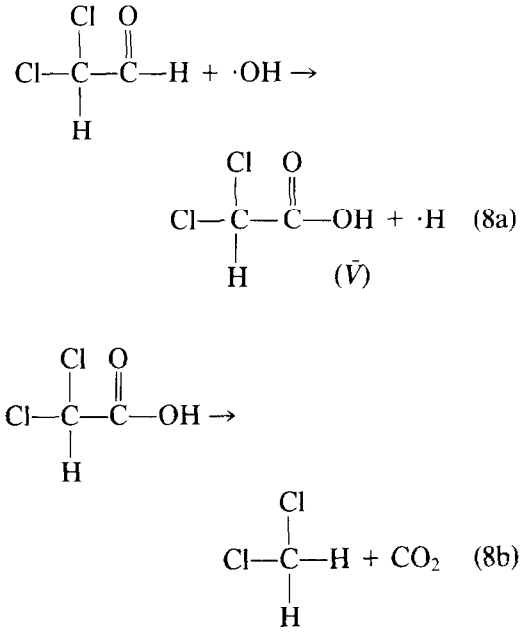

Krauetler and Bard have observed the decomposition of organic acids to CO_2 and the corresponding alkanes in deaerated aqueous suspensions of TiO_2 under uv-illumination (*45*). Traces of molecular hydrogen were also observed. We have confirmed methane and carbon dioxide production in the decomposition of acetic acid in this laboratory (*17*). Thus, the decomposition of the acid suggested in Eq. (8b) is feasible. Since alcohol hydroxyls appear to bind more strongly on TiO_2 than aldehydes or ketones (*4*), a strong binding caused by the acid hydroxyl could explain why the acid was not observed in solution.

The details of the continued degradation reaction are unclear; it is likely that continued attack by hydroxyl groups occurs. Phosgene ($COCl_2$) and chloroform ($CHCl_3$) have been observed in the vapor phase reaction between ·OH and tetrachloroethylene (*53*). Since phosgene decomposes rapidly in water

$$COCl_2 + H_2O \rightarrow CO_2 + 2HCl \quad (9)$$

and chloroform is converted under our reaction conditions to CO_2 and chloride ion (*10*), neither phosgene nor the Cl_2CH_2 product suggested in Eq. (8a,b) would be observed in the illuminated TiO_2 slurry.

Subsequent experiments in our laboratory (*60*) have demonstrated that the presence of molecular oxygen is *required* for the continual, *complete* mineralization of trace partially chlorinated hydrocarbons to CO_2 and HCl. The corresponding stoichiometry for trichloroethylene mineralization to CO_2 and HCl is given by Eq. (10).

$$CCl_2CClH + H_2O + \tfrac{3}{2}O_2 \rightarrow 2CO_2 + 3HCl \quad (10)$$

Although air was not purged through the liquid during these experiments, molecular oxygen may have entered by two routes. First, at the time of addition of fresh liquid, or of catalyst, replacement of the helium headspace vapor by air (see Fig. 1, sampling vessel) would have provided sufficient oxygen for Eq. (10). Additional molecular oxygen may have been supplied by the Teflon tubing, since this material may dissolve molecular oxygen. Subsequent experiments with an all glass recirculation loop (*60*) have verified the need for molecular oxygen in Eq. (10), and these are reported in a companion paper. We note again that the closure obtained on the chlorine balance (Table 1), the lack of any intermediates other than DCA, and the establishment of CO_2 production (by $Ba(CO_3)_2$ formation) verifies that total mineralization to CO_2 and HCl was obtained here, as indicated by Eq. (10).

Theoretically, a mass balance can be written for mineralization of trichloroethylene using water as an oxidant (Eq. (11)).

$$CCl_2CClH + 4H_2O \rightarrow 2CO_2 + 3HCl + 3H_2 \quad (11)$$

Conversion of 50 ppm TCE according to Eq. (11) would produce 2.25 ppm H_2, corresponding to about 16 ml of this nearly insoluble gas. The lack of observed gas evolution when 50 ppm or more TCE was converted to CO_2 and HCl, in the system of Fig. 1 or in an all glass system (*60*), indicates clearly that Eq. (11) is not a major reaction. (The chlorinated hydrocarbon may be attacked by the photoactive surface, in the absence of oxygen, but the reaction is self-poisoning; the inhibition is eliminated by subsequently supplying molecular oxygen (*60*).

CONCLUSIONS

(1) We have demonstrated the complete degradation of trichloroethylene and dichloroacetaldehyde by photoassisted heterogeneous catalysis over titanium dioxide, and identified the major products as the inorganic species carbon dioxide and chloride ion.

(2) We have determined reaction rates quantitatively with respect to both catalyst surface area and illumination intensity. The turnovers accomplished for TCE indicate that this conversion is a catalytic reaction. A rate expression accounting for the inhibitory effect of chloride on TCE disappearance was presented, and the chloride and TCE adsorption coefficients were calculated.

(3) We have suggested a mechanism for the formation of dichloroacetaldehyde which invokes observed intermediates and accounts for the participation of photogenerated holes and electrons in the reaction. A reaction which rationalizes the carbon–carbon bond breaking step, required for CO_2 production, was also suggested.

Finally, we note again that a potential exists for the application of heterogeneous photoassisted catalysis in removal of chlorinated hydrocarbons such as TCE (present work) and chloroform (*10*) from water. The reaction conditions are mild, the reaction times modest, and of greater importance, the reaction products are innocuous inorganic species.

ACKNOWLEDGMENTS

We thank the National Science Foundation and the Engineering Foundation for research support. Ann L. Pruden also thanks Mobil Oil for a Mobil Incentive Fellowship during most of this study.

REFERENCES

1. Symons, J. M., *et al., J. Amer. Water Works Assoc.* **67,** 634 (1975).
2. Foley, P. D., and Missingham, G. A., *J. Amer. Water Works Assoc.* **68,** 105 (1976).
3. Rook, J. J., *J. Amer. Water Works Assoc.* **68,** 168 (1976).
4. "Annual Report on Carcinogenesis Bioassay of Chloroform," National Cancer Institute, Bethesda, Md., March 1, 1976.
5. Stein, M. W., and Sansome, F. B., "Degradation of Chemical Carcinogens," pp. 116. Van Nostrand Reinhold, New York, 1980.
6. Streir, M. P., *Environ. Sci. Technol.* **14,** 28 (1980).
7. Rook, J. J., *Water Treat. Exam.* **23,** 234 (1974).
8. Sax, N. I., "Dangerous Properties of Industrial Materials," 3rd ed., p. 550. Van Nostrand Reinhold, New York, 1968.
9. Childs, L. P., and Ollis, D. F., "Heterogeneous Photoassisted Mineralization of Chloroform and Trichloroethylene in Water," Conference on Heterogeneous Catalysis in Atmospheric Chemistry, Albany, N.Y., June 1981.
10. Pruden, A. L., and Ollis, D. F., submitted for publication.
11. Carey, J. H., Lawrence, J., and Tosine, H. M., *Bull. Environ. Contam. Toxicol.* **16,** 697 (1976).
12. Childs, L. P., and Ollis, D. F., *J. Catal.* **66,** 383 (1980).
13. Oliver, B. G., Cosgrove, E. G., and Carey, J. H., *Environ. Sci. Technol.* **13,** 1075 (1977).
14. Gäb, S., Schmitzer, J., Tamm, H. W., Parlar, H., and Korte, F., *Nature* **270,** 331 (1977).
15. Calvert, J. J., and Pitts, J. N., "Photochemistry," p. 522. Wiley, New York, 1966.
16. Surface area determinations were performed by the Analytical Services Department, Mobil Research and Development Corporation, Paulsboro, N.J.
17. Spriegel, J. R., B.S.E. thesis, pp. 16, 72. Princeton University, 1979. X-Ray diffraction and analysis were performed by H. B. Barr, Department of Geology, Princeton University.
18. Dean, J. A. (ed.), "Lange's Handbook of Chemistry, 11th ed., p. 10. McGraw–Hill, New York, 1973.
19. Harbour, J. R., and Hair, M. L., *J. Phys. Chem.* **83,** 625 (1979).
20. Dean, J. A. (ed.), "Lange's Handbook of Chemis-

try," 11th ed., p. 4. McGraw–Hill, New York, 1973.
21. The activity spectrum of TiO_2 for alkane oxidation reactions closely parallels the uv-absorption spectrum; i.e., there is no reaction without photon absorption by the solid.
22. The Beer–Lambert relation defines the absorbance in terms of initial and transmitted intensities as $A = \log(I_0/I) = ECX$, where the product of E, the molar extinction coefficient, C, the concentration of absorbing species, and X, the path length, is a dimensionless quantity.
23. Hatchard, C. G., and Parker, C. A., *Proc. Roy. Soc. London, Ser. A* **235,** 518 (1956).
24. Murov, S. L., "Handbook of Photochemistry," p. 122. Dekker, New York, 1973.
25. Piet, G. J., Slingerland, P., deGrunt, F. E., van den Heuvel, M. P. M., and Zoeteman, B. C. J., *Anal. Lett. A* **11**(5), 437 (1978).
26. Kolthoff, I. M., and Sandell, E. B., "Textbook of Quantitative Analysis," 3rd ed., p. 542ff. MacMillan Co., New York, 1952.
27. Taras, M. J., *et al.* (eds.), "Standard Methods for the Examination of Water and Wastewater," 13th ed., p. 96ff. Amer. Public Health Assoc., New York, 1971.
28. The loan of this instrument by J. J. Kolsted and J. M. Calo is gratefully acknowledged.
29. The assistance of Dr. M. Miller and the Analytical Services Department, Mobil Research and Development Corporation, Paulsboro, N.J., in the GC-MS determinations is gratefully acknowledged.
30. Brammel, C. F., and Tseung, A. C. C., "3rd International Conference on Photochemical Conversion and Storage of Solar Energy, Boulder, Colorado, 1980," 355.
31. Nozik, A. J., Boudreaux, D. S., and Chance, R. R., *in* "Interfacial Photoprocesses: Energy Conversion and Synthesis" (M. S. Wrighton, ed.), Advances in Chemistry, Vol. 184, pp. 155. Amer. Chem. Soc., Washington, D.C., 1980.
32. Herrmann, J. M., and Pichat, P., *J. Chem. Soc. Faraday Trans. 1* **76,** 1138 (1980).
33. Childs, L. P., Ph.D. thesis, Princeton University, 1981.
34. Lo, W. J., Chung, Y. W., and Somorjai, G. A., *Surf. Sci.* **71,** 199 (1978).
35. Gravelle, P. G., Juillet, F., Meriaudiau, P., and Teichner, S. J., *Disc. Faraday Soc.* **52,** 140 (1971).
36. Gates, B. C., Katzer, J. R., and Schuit, G. C. A., "Chemistry of Catalytic Processes," p. 150. McGraw–Hill, New York, 1979.
37. Morrison, R. T., and Boyd, R. N., "Organic Chemistry," 3rd ed., p. 260. Allyn & Bacon, Rockleigh, N.J., 1973.
38. Carrizosa, I., and Munuera, G., *J. Catal.* **49,** 174 (1977).
39. Carrizosa, I., and Munuera, G., *J. Catal.* **49,** 189 (1977).
40. Kaliaguine, S. L., Shelimov, B. N., and Kazansky, V. B., *J. Catal.* **55,** 384 (1978).
41. Childs, L. P., and Ollis, D. F., *J. Catal.* **67,** 35 (1981).
42. Kraeutler, B., and Bard, A. J., *J. Amer. Chem. Soc.* **100,** 5985 (1978).
43. Kraeutler, B., Jaeger, C. D., and Bard, A. J., *J. Amer. Chem. Soc.* **100,** 4903 (1978).
44. Morrison, S. R., "The Chemical Physics of Surfaces," p. 118. Plenum, New York, 1977.
45. Cundall, R. B., Rudham, R., and Salim, M. S., *J. Chem. Soc. Faraday Trans. 1* **72,** 1642 (1976).
46. Bickley, R. I., and Stone, R. S., *J. Catal.* **31,** 389 (1973).
47. Bickley, R. I., and Vishnawathan, V., *Nature (London)* **280,** 306 (1979).
48. Pappas, S. P., and Fischer, R. H., *J. Paint Technol.* **46,** 65 (1974).
49. Volz, H. G., Kampf, G., and Fitsky, H. G., *Farbe Lack.* **78,** 1937 (1972).
50. Jaeger, C. D., and Bard, A. J., *J. Phys. Chem.* **83,** 3146 (1979).
51. Bamford, C. H., and Tipper, C. F. H. (eds.), "Comprehensive Chemical Kinetics," Vol. 20, "Complex Catalytic Processes," pp. 300, 332. Elsevier, Amsterdam, 1978.
52. Huntress, E. M., "The Preparation, Properties, Chemical Behavior and Identification of Chlorine Organic Compounds: Tables of Data on Selected Compounds of Order III," p. 611. Wiley, New York, 1948.
53. Crosby, D. G., University of California, Davis, personal communication, Sept. 4, 1980.
54. Boonstra, A. H., and Mutsaers, C. A. H. A., *J. Phys. Chem.* **79,** 1694 (1975).
55. Herrmann, J. B., Disdier, J., and Pichat, P., *in* "Proceedings, 7th Int. Vac. Congr. and 3rd Int. Conf. Solid Surfaces, Vienna, 1977" (R. Dobrozemsky *et al.*, eds.), p. 951.
56. Herrmann, J. M., Disdier, J., Mozzanega, M-N., and Pichat, P., *J. Catal.* **60,** 369 (1979).
57. Kraeutler, B., and Bard, A. J., *J. Amer. Chem. Soc.* **100,** 2239, 5985 (1978).
58. Boonstra, A. H., and Mutsaers, C. A. H. A., *J. Phys. Chem.* **79,** 2025 (1975).
59. van Damme, H., and Hall, W. K., *J. Amer. Chem. Soc.* **101,** 4373 (1979).
60. Hsiao, C.-Y., Lee, C.-L., and Ollis, D. F., *J. Catal.* **82,** 1983.